ESTABLISHMENT OF AN IN VIVO MODEL OF HUMAN PANCREATIC TUMOR FOR PRECLINICAL STUDIES AND EVALUATION OF RADIOIODINATED PHENYLALANINE-ANALOGUES AS RADIOPHARMACEUTICALS TO IMAGE PANCREATIC CARCINOMAS

S. Samnick [1], D. Hellwig [1], B.F. Romeike [2], G. Schneider [3], M. Menger [4], C.M. Kirsch[1]

Departments of [1]Nuclear Medicine, [2]Neuropathology, [3]Experimental Radiology, [4]Clinical Experimental Surgery, Saarland University Medical Center, D-66421 Homburg/Saar, Germany. e-mail: rassam@uniklinik-saarland.de

Keywords: In vivo model, pancreatic carcinomas, Noninvasive imaging, SPET

Adenocarcinoma of the pancreas is one of the least understood and most incurable malignancies. Almost all patients with this disease die within 1 year of diagnosis. To facilitate development of novel radiopharmaceuticals for diagnostic and therapeutic uses, in vivo models are need that closely mimic the natural biological behaviour of pancreatic carcinomas in humans. This work aimed to establish an in vivo model of human pancreatic cancer for this purpose and to evaluate the potential of the pancreatic carcinoma-affine L-p-amino-3-[^{123}I]Iodo-phenylalanine (IAPA) and L-p-[^{123}I]Iodo-phenylalanine (IPA) preclinically.

The human pancreatic carcinomas, PaCa44 and PanC1 (1-2 x 10^6 cells in 10-30 microL PBS), were implanted either subcutaneously into the flank or orthotopically into the pancreas of anesthesized severe combined immunodeficient (SCID) mice. The size of sc. tumor was recorded twice weekly using linear calipers. Additionally, tumor formation was monitored noninvasively by MRI, using a small animal magnetic resonance tomograph, as well as histopathologically after biodistribution and SPET studies with IPA and IAPA.

All animals developed a pancreatic tumor within 3.5 weeks. The tumor was clearly demonstrated in all animals with subcutaneous implantation by MRI, as well as 90%, and 60% of the orthotopic implanted PaCa44 and PanC1 cells, respectively. No invasion or metastases could be demonstrated by heterotropic-implanted tumors. Tumor growth and spread following orthotopic implantation resembled the situation in human, including invasion into adjacent organs and metastases formation in different sites in the abdomen, especially in mice bearing PaCa44 cells.

Biodistribution study followed i.v. application revealed that IPA and IAPA were excreted by urine. Moreover, both radioligands showed high tumor uptake. Radioactivity accumulation in tumor, 60 and 240 min p.i. amounted 8,6 and 6,1 %I.D./g for IAPA, and 12 and 16,7 %I.D./g for IPA, respectively, with tumor-to-organ ratios of 1,1 - 4,2 (Tu/blood), 1,4 - 5,4 (Tu/Liver), 2,1 - 5,5 (Tu/spleen) and 3,3 - 11,7 (Tu/Muscle). In comparison tumor uptake following FDG injection was 15,5 and 3,5 %I.D./g. However, organ uptakes in both implantations provided evidence that the orthotopic transplant model more than the heterotopic one appropriately reflects the entire process of human pancreatic cancer.

The present cancer model is a powerful tool for biological studies of human pancreatic tumor and for preclinical evaluations of radiopharmaceuticals. Moreover, results of biodistribution studies suggest that IAPA and IPA are very interesting candidates as radiotracers for noninvasive imaging of pancreatic carcinomas by SPET.

MULTI-MODALITY IMAGING STUDIES ON OSTEOLYTIC BONE METASTASIS

X. Sun[1], S.J. Bakewell[2], J.R. Garbow[3,4], K.M. Gauvain[3], J.S. Lewis[1,4], J.R. Rutlin[1], K.N. Weilbaecher[2,4], C.J. Anderson[1,4] and M.J. Welch[1,4]

[1]Mallinckrodt Institute of Radiology, 510 S. Kingshighway Blvd.; [2]Department of Internal Medicine, Division of Oncology, 216 Kingshighway; [3]Biomedical MR Laboratory, 4525 Scott Ave.; [4]the Alvin J. Siteman Cancer Center. Washington University School of Medicine, St. Louis, MO 63110. E-mail: sunx@mir.wustl.edu

Keywords: microPET, MRI, FDG, bone metastasis

Introduction. Bone is the most common site for metastasis in a variety of cancers, including breast, prostate, melanoma, and lung cancer. Breast and prostate cancers account for over 80% of cases of metastatic bone disease, show the highest prevalence in bone metastasis, and cause the greatest morbidity due to intractable bone pain, pathological fractures, hypercalcemia and nerve compression (1). Bone metastasis is only detectable by X-ray or ^{99m}Tc scintigraphy when lesions are quite advanced. Thus, it is of great significance to develop methods for the early detection and mechanistic understanding of bone metastases. In this study, we employed both microPET and MR imaging modalities for this purpose using an osteolytic bone metastasis model (2).

Methods. B16 Mouse Melanoma cells were a gift from Dr. David Fisher, Dana Farber Cancer Center (Boston, MA). The tumor cells (1×10^4 suspended in 50 L PBS) were injected into the left tibia of C57bl6/129 male and female mice aged between 6 to 8 wk, with the right tibia serving as an internal control. MR imaging and ^{18}F-FDG microPET were carried out on the mice (n = 4) at 3, 7, 11, 14, 17(18, MR) and 21 d after tumor injection. MR images were collected using an Oxford Instruments 4.7 tesla magnet equipped with 10-cm, inner-diameter, actively shielded gradient coils (maximum gradient 60 G/cm, 200 sec rise time). For each mouse, multi-slice, T2-weighted transaxial spin-echo images were collected of both the right and left tibia. The magnet/gradients are interfaced with a Varian (Palo Alto, CA) INOVA console, and data were collected using a homebuilt 2.5-cm birdcage rf coil. PET imaging was performed on the first commercially available microPET (Concorde Microsystems, Knoxville, TN). ^{18}F-FDG (*ca.*100 Ci) was injected *via* the tail vein, and the images were obtained at 1 h p.i. The regions of interest (ROI) with the average radioactivity concentration in the targeted organ were chosen for the standardized uptake value (SUV) analysis.

Results and discussion. From the quantitation of the microPET images, the SUV ratio of the left tibia to the right tibia (LT/RT_{suv}) was calculated as follows (n = 4): 1.10 0.26 (3 d); 1.13 0.21 (7 d); 1.32 0.21 (10 d); 1.38 1.26 (14 d); 2.12 1.08 (17 d); and 2.56 1.78 (21 d). Despite the relatively large standard deviations due to the small sampling, the analysis exhibited a clear trend: LT/RT_{suv} increased as the tumor inside the left tibia grew and metastasized. This observation was confirmed by the MR images, which showed no visible tumor at 3 d, but revealed bone marrow infiltration of tumor in all mice between days 7 and 14. Furthermore, the MR images unequivocally demonstrated that tumors broke through the cortex and invaded the soft tissue of the leg between days 11 and 18. By enabling *in-vivo* measurement of tumor volumes, MR imaging allowed the progression of these bone tumors to be monitored quantitatively. These results demonstrate that both microPET and MR imaging modalities can be employed to monitor bone metastasis from a very early stage, and can provide information about the proliferation of the bone metastases. The imaging techniques developed in this study can also be used to monitor therapy for bone metastasis.

Acknowledgment. The authors would like to thank Nicole Mercer and John Engelbach for technical assistance. MicroPET and MRI imaging is supported by an NIH/NCI SAIRP grant (1 R24 CA83060) with additional support from the Small Animal Imaging Core of the Alvin J. Siteman Cancer Center (NCI Cancer Center Support Grant # 1 P30 CA91842). The production of ^{64}Cu is supported by NCI R24 CA86307.

1. Coleman R E. *Cancer Treat Rev* 2001; 27: 165-176
2. Arguello F, Baggs R B, Frantz C N. *Cancer Res* 1988; 23: 6876-81

MICROPET IMAGING OF THE EFFECTS OF TUMORCIDAL 2-DEOXYGLUCOSE

J.S. Lewis[1,3], R.L. Aft[2,3], F. Zhang[2], J. Kim[1] and M.J. Welch[1,3]

[1]Division of Radiological Sciences, Mallinckrodt Institute of Radiology, [2]Department of Surgery and the [3]Alvin J. Siteman Cancer Center, Washington University School of Medicine, St. Louis, MO, 63110, USA *Contact:* Jason S. Lewis, Mallinckrodt Institute of Radiology, Washington University School of Medicine, Campus Box 8225, 510 S. Kingshighway Blvd. Saint Louis, MO 63110, USA. Email: lewisjas@mir.wustl.edu

Keywords: Cu-ATSM, microPET, 2DG, hypoxia

Many solid tumors have hypoxic regions due to aberrant vascularization. This results in heterogeneous distribution of drug levels. Previously tested radiosensitizers have been limited by their clinical toxicity and lack of clinical effectiveness. 2-deoxyglucose (2DG) has been shown to potentiate the cytotoxic effect of ionizing radiation and certain chemotherapeutic agents (1, 2). Since 2DG becomes selectively trapped within cancer cells, it should differentially sensitize tumor cells while sparing or having a lesser effect on normal tissues. Using microPET we have endeavoured to elucidate the mechanism of 2DG. Also in this series of experiments, we have tested the efficacy of combining two tumor-specific cytotoxic agents in a mouse model of breast cancer to develop a targeted therapy for breast tumors. We first determined the optimal method of administering 2DG via ^{18}F-FDG-MicroPET. 2-DG was mixed with ^{18}F-FDG, given intra-gastric (IG), IV, IP or subcutaneously to mice. Distribution of the ^{18}F-FDG was determined at 1 hour and 3 hours after administration. MicroPET imaging demonstrating that 2DG/^{18}F-FDG uptake at 3 hours varies according to the mode of administration (IP, IV, sub-q, IG). Quantification of the microPET data demonstrates that IP = IV for ^{18}F-FDG distribution at both 1 and 3 hours. MicroPET imaging was performed using ^{18}F-FDG to determine whether uptake of 2DG changed over time of treatment. Mice bearing EMT-6 tumors were treated with 40 mg/mouse (2 mg/kg) and imaged on days 1, 7, 11, 14. ^{18}F-FDG uptake by tumors was stable for the duration of the treatment, indicating that resistance to uptake of 2-DG does not develop. Brain uptake decreased slightly with 2-DG treatment. This could indicate either a change in metabolism by the brain tissue or a saturation of the transporters. We next determined the effect of 2-DG on tumor uptake of ^{64}Cu-ATSM (hypoxia) and ^{64}Cu-PTSM (flow) using microPET imaging. Mice were given 2-DG on the day of the scan and one day prior to the scan. Analysis of the data using ^{64}Cu-PTSM, showed a rapid uptake of ^{64}Cu-PTSM by all tumors. When ^{64}Cu-ATSM was used as the tracer uptake increased with 2DG treatment. A dose dependent increase in uptake and retention was observed in the tumor with 2DG treatment. This is in contrast to normoxic brain tissue which rapidly accumulates and releases ^{64}Cu-ATSM and is relatively unaffected by 2DG treatment. This effect of 2-DG was observed only for the hypoxia-specific agent ^{64}Cu-ATSM and not with the non-hypoxia selective agent ^{64}Cu-PTSM. Our experiments demonstrate that 2DG treatment results in increased uptake and retention of ^{64}Cu-ATSM by EMT6 mouse breast cancer tumors. In therapy studies when 2-DG was combined with a single dose of ^{64}Cu-ATSM (2 mCi), tumor growth was inhibited approximately 60% compared to untreated mice and animals survived approximately 50% longer than untreated mice or animals treated with each agent alone (32 versus 20 days). From our microPET imaging we hypothesize that 2DG alters the redox state of the cell creating a functional hypoxia within normoxic areas of tumors leading to increased uptake of ^{64}Cu-ATSM. This would result in a uniform high local dose of radiotherapy. This work was financially supported by the US Department of Energy (DE-FG02-87ER60212) and an AWS/Ethicon Grant. MicroPET imaging is supported by an NIH/NCI SAIRP grant (1 R24 CA83060) with additional support from the Alvin J. Siteman Cancer Center at Washington University. The SAIC Core is supported by an NCI Cancer Center Support Grant # 1 P30 CA91842. The production of ^{64}Cu is supported by NCI R24 CA86307.

1. Aft R, Zhang F, Gius, D. *British Journal of Cancer*, *87:* 805-812, 2002.
2. Lin X, Zhang F, Bradbury M, Kaushal A, Spitz D, Aft R, Gius, D. *Cancer Research*, 2003

ORANOMETALLIC RE- AND ^{99m}TC-TRICARBONYL-COMPLEXES OF THYMIDINE ANALOGUES: SYNTHESIS, STRUCTURE-ACTIVITY RELATIONSHIPS, AND BIOLOGICAL EVALUATION

M.Netter[1], R.Schibli[1], L.Scapozza[2], A.Schubiger[1]

[1] Centre of Radiopharmaceutical Science, PSI, Villigen, [2] Department of Pharmacy, ETH, Zurich, Switzerland

Keywords: Thymidine kinase, organometallic, technetium-99m, rhenium, thymidine analogues, molecular modelling

C-11-thymidine and the thymidine (dT) analogues Br-76-fluoro-desoxyuridine (Br-76-BFU) and F-18-desoxy-fluorothymidine (F-18-FLT) are used for imaging of tumour proliferation via PET (1, 2). More recently PET labelled dT analogues are under consideration for monitoring the viral replication and the tumour response to therapy in "suicide gene therapy". Thus there is a high potential of inexpensive ^{99m}Tc based thymidine analogues for both applications.

In this study we present the first synthesis of organometallic rhenium/technetium based thymidine analogues for use in gene therapy monitoring and for tumour proliferation. Our synthetic strategy was guided by structures of potent antiviral nucleoside analogues (K_i values in the nanomolar range) with bulky entity at the C5´ position (3). dT was derivatised at the C5´ and various spacers, namely propyl, butyl, heptyl, dodecyl and eicosyl spacers, were introduced between 5'-amino-dT and the metal chelating moiety. For tridentate coordination of the $[M(H_2O)_3(CO)_3]^+$(M = Re, ^{99m}Tc) fragment, a iminodiacetic acid chelating system was chosen (see figure). The corresponding organometallic thymidine complexes have been fully characterized by means of IR-, NMR-, mass-spectroscopy and HPLC. Internalization studies with four different cancer cell lines showed uptake of the ^{99m}Tc-$(CO)_3$-dT-complex of about 3±1.1% (Caki-2), 4.9±1.3% (GW), 3.6±1.1% (HT-29), and 8.9±3.2% (PC-3). However, the experiments indicated an uptake via passive diffusion and not via the nucleoside transport system (notabene: Azidothymidine, Zidovudine®, is also internalized via passive diffusion (4)). Enzyme kinetic studies revealed competitive inhibition exclusively of the human cytosolic thymidine kinase (hTK1) and not as expected for the Herpes Simplex virus thymidine kinase (HSV-1 TK). This is to our knowledge the first time such a "reversed" selectivity of a dT derivative is observed. We found a correlation between spacer lengths and the K_i values. Extensions of the spacer give raise to lower K_i values. Re$(CO)_3$-dT-complexes with spacers with n=3-14 showed inhibition exclusively towards hTK1 (see figure). Compounds with spacers with n>20 evinced inhibition of the HSV-1 TK. These results are supported by molecular modelling and homology studies, which indicated that significant structural differences near the 5' position of bounded dT (at the outer sphere of the active site) exists in human, cytosolic and HSV-1 TK. Recent docking results predict that Re(CO) 3-dT-complexes with short chains between the thymidine and the organometallic moiety might have high affinities towards the enzymes. Current studies are in progress. The potential of these ^{99m}Tc labelled thymidine complexes as proliferation markers in vivo is currently under investigation, as well as the optimization of the inhibitory activity and the selectivity against HSV-1 TK via synthesis of a 5-ethyl-uridine derivative.

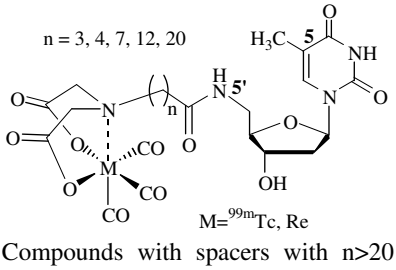

1. Mankoff DA, Shields AF, Graham MM, Link JM, Eary JF, Krohn KA. *J Nucl Med* 1998; 39: 1043-1055.
2. Borbath I, Gregoire V, Bergstrom M, Laryea D, Langstrom B, Pauwels S. *Eur J Nucl Med* 2002; 29: 19-27.
3. Martin JA. *Bioorg Med Chem Lett* 2001; 11: 1655-1658.
4. Ming H. *J Pharm Sci* 1993; 82: 829-833.

STEREOSPECIFIC SYNTHESIS AND BIOLOGICAL EVALUATION OF S/R-[^{123}I]IVAIB FOR BRAIN TUMOR IMAGING

W. Yu[1], J.McConathy[1], L.Williams[1], E.Malveaux[1], V.M.Camp[1], Z.Zhang[2], J.Olson[2], M.M.Goodman[1]

[1]Division of Radiological Sciences, Emory University, Atlanta, GA 30322
[2]Department of Neurosurgery, Emory University, Atlanta, GA 30322, wyu2@emory.edu

Key words: IVAIB, iodine-123, brain tumor imaging

Amino acids S/R-3(E)-2-amino-2-methyl-4-iodo-3-butenoic acid (S/R-IVAIB) were synthesized, [^{123}I]radiolabeled and evaluated as potential SPECT tumor imaging agents in rat 9L gliosarcoma tumor model. The required S/R-IVAIB precursors for radiolabeling were prepared as shown in Scheme 1. Radioiodination was carried out with no-carrier-added [^{123}I]NaI-H_2O_2/H^+. S/R-[^{123}I]IVAIB were obtained by hydrolysis with 4N hydrochloric acid and chromatographic purification. Radiolabeling yields were 72% (n=9, S[^{123}I]IVAIB) and 67% (n=8, R-[^{123}I]IVAIB), with radiochemical purity over 99% as measured by radiometric TLC for both isomers.

Scheme 1: The preparation of stannylated S/R-IVAIB precursors

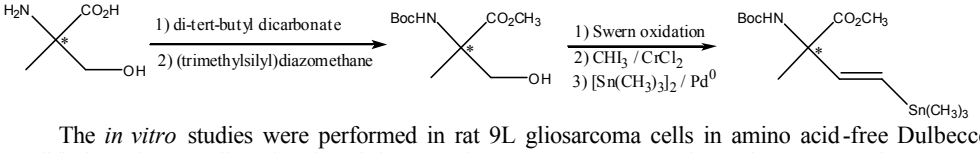

The *in vitro* studies were performed in rat 9L gliosarcoma cells in amino acid-free Dulbecco's Modified Eagle's Medium incubated for 30 minutes at 37 ºC to evaluate the compound's tumor cell uptake and transport mechanism. 10 mM 2-amino-bicyclo[2.2.1]-heptane-2-carboxylic acid and 10 mM N-methyl-a-aminoisobutyric acid were used as L- and A-type amino acid transporter inhibitors, respectively. The cell uptake was calculated in percent CPM per million cells. We found that the stereochemistry influenced substrate specificity of these amino acids thus S-IVAIB entered 9L tumor cells *in vitro* primarily *via* A-type amino acid transport, while R-IVAIB was an L-type candidate.

The *in vivo* biodistribution studies were carried out in Fischer rats with 9L tumors implanted intracranially. The radioactivity in tumors and in normal tissues of tumor-bearing Fischer rats (n=4-6 at each time point) was measured at 30, 60, 120 min *p.i.* Values were reported as mean percent dose per gram tissue. The distributions of radioactivity in tumor and in brain are listed in Table 1. The experiment showed that IVAIB had a rapid and prolonged accumulation in tumors. S- isomer gave a much higher tumor to brain ratio than R- isomer. Low uptake was found in heart, liver, lung, and thyroid. These results support the candidacy of S/R-[^{123}I]IVAIB as SPECT brain tumor imaging agents. S-IVAIB, an A-type amino acid transport ligand, may have greater potential than R-IVAIB, a L-type ligand, in imaging brain tumors. Research supported by Nihon Medi-Physics Co., Ltd.

Table 1: The tumor and brain distribution of [^{123}I]IVAIB in 9L tumor-bearing Fischer rats

	30 min.	60 min.	120 min.
S-[^{123}I]IVAIB			
Tumor	4.703	6.812	6.838
Brain	0.058	0.0912	0.0957
Tumor/Brain	81.1	74.7	71.5
R-[^{123}I]IVAIB			
Tumor	0.186	0.512	0.392
Brain	0.018	0.066	0.051
Tumor/Brain	10.3	7.74	7.68

SYNTHESIS OF F-18 LABELED GLYBURIDE ANALOGS AS b-CELL IMAGING AGENTS.

C-Y. Shiue[1], A. Schmitz[1], Q. Feng[1], A.A. Alavi[1], B.A. Wolf[2], R. Schirrmacher[3] and F. Rosch[3]

Departments of [1]Radiology and [2]Pathology, University of Pennsylvania, Philadelphia, PA. 19104, USA; [3]Institut fur Kernchemie, Johannes Gutenberg-Universitat, Mainz, Germany. Email: shiue@rad.upenn.edu.

Keywords: F-18 labeled glyburide, ß-cell imaging, PET, Diabetes

Diabetes mellitus is characterized by a deficiency in insulin secretion and -cell loss. A non-invasive method to monitor the status of -cells during the silent phase of prediabetes or after pancreas transplantation will be useful for the treatment of diabetes mellitus. The purpose of this study was to develop fluorinated glyburide analogs [2-fluoroethoxy (**3**), 2-fluoropropoxy (**4**), 2-fluorobutoxy (**5**), 2-*p*-fluorobenzyl-5-chloro-glyburide (**6**) and their 5-iodo analogs (**7-10**)] (Figure 1), and study their structure-activity relationships as insulin secretagogues and -cell imaging agents.

Compounds **3-6** and **7-10** were synthesized in multi-steps from 5-chloro- and 5-iodosalicylic acid, respectively, with the appropriate fluoroalkyl bromide or tosylate in ~ 10% yield. The precursors for F-18 labeling, namely 2-hydroxy-5-chloroglyburide (**1**) and its iodo analog (**2**) were synthesized from 5-chloro- and 5-iodosalicylic acid, respectively. The F-18 labeled **3-5** and **7-9** were synthesized by alkylation of **1** and **2**, respectively, with the appropriate F-18 labeled fluoroalkyl tosylate followed by purification with HPLC in 5-10% yield in a synthesis time of 120 min from EOB. These compounds were evaluated as insulin secretagogues and -cell imaging agents. For insulin secretion, 100 rat islets were pre-perifusion in perifusion solution with no substrate added for 30 min followed by **3-10** RAMP (50 nM/min to 2 M) for an additional 30 min. Insulin in the efflux samples was determined using RIA procedure. The results showed that compounds **3-10** all stimulate insulin release from rat islets with compounds **6** and **10** being the highest. The *in vitro* binding affinities of F-18 labeled **3-5** and **7-9** to whole -cells (TC3 and Min 6) were determined by incubating F-18 labeled glyburide analogs and non-radioactive counterparts (1-10,000 nM) with monolayer -cells at 25^{0}C for 1 h followed by separation and counting in a counter. The results showed that up to 2% of F-18 radioactivity was bound to -cells and that the binding of compounds **4, 5, 8, 9** to -cells was less saturable compared to compounds **3** and **7**.

In conclusion, this study shows that increasing the length of the side chain of the fluorinated glyburide analogs resulted in an increase of their non-specific binding to whole -cells and that F-18 labeled compounds **3, 7** and **6, 10** may serve as -cell imaging agents.

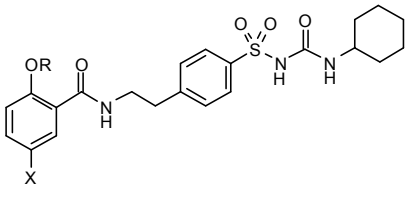

1). X=Cl, R=H; 6). X=Cl, R=CH_2-*p*-F-C_6H_5
2). X=I, R=H; 7). X=I, R=$(CH_2)_2F$;
3). X=Cl, R=$(CH_2)_2F$; 8). X=I, R=$(CH_2)_3F$;
4). X=Cl, R=$(CH_2)_3F$; 9). X=I, R=$(CH_2)_4F$;
5). X=Cl, R=$(CH_2)_4F$; 10). X=I, R=CH_2-*p*-F-C_6H_5

Figure 1.

THE IMPORTANCE OF LYMPHOSCINTIGRAPHY IN SENTINEL NODE BIOPSY FOR MELANOMA AND BREAST CANCER

R.F. Uren MD, FRACP, DDU.
Nuclear Medicine and Diagnostic Ultrasound, RPAH Medical Centre, The Sydney Melanoma Unit, Royal Prince Alfred Hospital, Sydney, NSW, Australia and The Department of Medicine, The University of Sydney, Sydney, NSW, Australia.

Lymphoscintigraphy(LS) using radio-labelled colloids to examine the lymphatic system was described 50 years ago. Since then it has been used in the occasional patient with lymphedema and prior to 1990 there had been some attempts to apply this technique to improve the management of patients with breast cancer and melanoma but these did not find general application. Most centres performed no more than 20 to 30 studies a year and the test was so rarely used than in the USA in the late 1980's one could have obtained the licence to manufacture 99mTc antimony sulphide colloid for a mere $10,000.

This all changed in 1990 when Don Morton and colleagues at the John Wayne Cancer Institute in Santa Monica described the technique of sentinel lymph node biopsy(SLNB) in melanoma patients. Their original method used injections of blue dye around the tumour site and intricate surgery which followed theblue dye through the draining lymphatic vessel to the first node it met, the sentinel node. They found that careful histological examination of this 1 node accurately staged the whole node field. The procedure was simplified by the use of pre-operative LS that showed the exact location and number of sentinel nodes before surgery. This greatly improved SLNB and standard practice now uses a combination of pre-operative LS, blue dye injection and the intra-operative use of a gamma-detecting probe.

This new use of an old technology, LS, has completely changed the importance of LS in most nuclear medicine departments and in my own practice we now perform about 600 studies a year on patients with melanoma and breast cancer. The use of this "old" technology on such a large number of patients has also had some suprising results. Since the aim of LS in SLNB is to provide an accurate map of the pattern of lymphatic drainage from the tumour site and to precisely mark the surface location of each SN on the skin, imaging protocols can no longer be routine and the imaging must be tailored to each individual patient until all SNs in each patient are defined.

The result of this has been a redefinition of the patterns of lymphatic drainage of the skin. Teachings on lymphatic drainage that have been standard for 150 years have been found incorrect and new pathways for lymph to flow from the skin have been defined including direct drainage through the body wall to SNs in the retroperitoneal, para-aortic and paravertebral areas. Lymph can also flow from the base of the neck up to nodes high in the cervical region or to occipital nodes. Flow across the mid-line is common and flow from the back often occurs over the shoulders to neck nodes and also to the triangular intermuscular space, a regional not previously known to drain the skin. Lymph flow can bypass whole node fields and flow to sentinel nodes in multiple node fields is not uncommon. This detailed study of lymphatic flow in each patient has allowed new incites into lymphatic physiology. It has been found that the speed of lymphatic flow varies in different parts of the body in a systematic way and that the most rapid flow is from the leg and foot.

In the breast LS for SLNB has reconfirmed previous studies which show that breast lymph flows not just to SNs in the axilla but to nodes in the internal mammary chain, supraclavicular region, interpectoral nodes and intra-mammary interval nodes. Such drainage to SNs outside the axilla is more common than previously thought and in my practice is seen in 46% of patients with breast cancer. Lymphatic drainage patterns from the breast are not predictable clinically based on the location of the tumour in the breast and unexpected drainage across the centre-line of the breast to axilla or internal mammary nodes occurred in 46% of patients. LS allows all true SNs to be located in every patient with

breast cancer. SLNB in breast cancer is moving towards biopsy of all SNs in each patient with breast cancer, and not just those SNs found in the axilla.

Sometimes in medicine it simply requires an "old" technique to be used in a new way to significantly change patient management for the better.